Acta Pharmaceutica Sinica B 2024;14(7):3140–3154

Chinese Pharmaceutical Association
Institute of Materia Medica, Chinese Academy of Medical Sciences

Acta Pharmaceutica Sinica B

www.elsevier.com/locate/apsb
www.sciencedirect.com

ORIGINAL ARTICLE

Selectively T cell phosphorylation activation of azvudine in the thymus tissue with immune protection effect

Ning Sheng [a,†], **Rui Li** [b,†], **Yang Li** [a], **Zhe Wang** [a], **Lulu Wang** [b], **Yuhuan Li** [b], **Jinlan Zhang** [a,*], **Jiandong Jiang** [a,b,*]

[a]*State Key Laboratory of Bioactive Substance and Function of Natural Medicines, Institute of Materia Medica, Chinese Academy of Medical Sciences and Peking Union Medical College, Beijing 100050, China*
[b]*Institute of Medicinal Biotechnology, Chinese Academy of Medical Sciences and Peking Union Medical College, Beijing 100050, China*

Received 4 December 2023; received in revised form 15 March 2024; accepted 27 March 2024

KEY WORDS

Azvudine;
T cell;
Thymus;
Phosphorylation activation;
Nucleoside analogue

Abstract Thymus is the important immune organ, responsible for T cell development and differentiation. The lower circulating T counts have been observed in patients who died from COVID-19 compared with survivors. Azvudine, also known as FNC, is a thymus-homing anti-SARS-CoV-2 drug in treating COVID-19 patients. In this study, single-cell transcriptome, proteomics, and parallel reaction monitoring (PRM) were applied to insight into the activation process of FNC in rat and SARS-CoV-2 rhesus monkey thymus. The results indicated that thymic immune cells possess a robust metabolic capacity for cytidine-analogue drugs such as FNC. Key enzymes involved in the FNC phosphorylation process, such as Dck, Cmpk1, and Nme2, were highly expressed in CD4+ T cells, CD8+ T cells, and DP (CD4+ CD8+) cells. Additionally, FNC could upregulate multiple phosphorylated kinases in various cell types while downregulating the phosphatases, phosphoribosyl transferases, and deaminases, respectively. The robust phosphorylation capacity of the thymus for cytidine analogue drug FNC, and the activation effect of FNC on the NAs metabolism system potentially contribute to its enrichment in the thymus and immune protection effect. This suggests that it is crucial to consider the expression level of phosphorylation kinases when evaluating NA drug properties, as an important factor during antiviral drug design.

*Corresponding authors.
E-mail addresses: zhjl@imm.ac.cn (Jinlan Zhang), jiang.jdong@163.com (Jiandong Jiang).
†These authors made equal contributions to this work.
Peer review under the responsibility of Chinese Pharmaceutical Association and Institute of Materia Medica, Chinese Academy of Medical Sciences.

https://doi.org/10.1016/j.apsb.2024.03.032

1. Introduction

The thymus serves as a vital immune organ and endocrine gland, playing a crucial role in the maturation of immunocompetent T cells that serve as the defense against various pathogens, including viruses and bacteria. For this purpose, T cells undergo positive and negative selection to eliminate non-functional and self-reactive T cells in the thymus[1]. Severe acute respiratory syndrome coronavirus 2 (SARS-CoV-2) can enter into T cells and dysregulate associated immune response by integrins acting as SARS-CoV-2 receptors on T cells[2,3]. Clinical studies have shown T-cell infection by SARS-CoV-2 and associated immune responses are related to disease severity and prognosis of coronavirus disease 2019 (COVID-19). The lower circulating T counts have been observed in patients who died from COVID-19 compared with survivors[4,5]. It has been reported that SARS-CoV-2 can infect thymus T cells, so the treatment of COVID-19 should both suppress the virus and protect thymus immune cells.

Our previous studies have indicated that 2′-deoxy-2′-β-fluoro-4′-azidocytidine (Azvudine, FNC) is a thymus-homing anti-SARS-CoV-2 drug effective in treating COVID-19 patients at 5 mg dose, and the active triphosphorylated metabolite (FNC-TP) was only detected in the thymus[6]. FNC, as a cytidine analogue of a synthetic viral RNA-dependent RNA polymerase (RdRp), is metabolized intracellularly into an active 5′-triphosphate metabolite. This activator can act specifically on RdRp, embedding viral RNA during SARS-CoV-2 RNA synthesis[7]. Thus, inhibiting SARS-CoV-2 replication, to achieve the role of COVID-19 treatment. The National Medical Products Administration (NMPA) of China has currently cleared FNC for emergency evaluation for common COVID-19. In animal models of SARS-CoV-2 infection, FNC significantly reduced the COVID-19 viral loads, improved the lymphocyte profile, reduced organ damage and inflammation, protected the immune function of the thymus, and quickly cured COVID-19.

The therapeutic activity of nucleoside analogues (NAs) depends largely on their efficient conversion to pharmacologically active phosphorylated forms. Many cellular factors are likely to impact this process, *e.g.*, cell type, cell cycle, activation state, and infection status[8,9]. NAs use the same metabolic pathways as natural nucleosides to reach their corresponding triphosphate active forms. After entry into the cell, antiviral NAs are converted into triphosphates by three successive reactions catalyzed by enzymes from the salvage pathway (nucleoside kinases, NMP kinases, and NDP kinase)[10–12]. On the contrary, their dephosphorylation process by such as cytosolic 5′-NT, and phosphoribosyl transferase may reduce their efficiency by increasing the relative concentrations of the inactive by-products compared to the active triphosphate counterparts[13,14]. The thymus is a vital immune organ. Previous studies have demonstrated the accumulation of the active 5′-triphosphate metabolite of FNC in thymus tissue, which effectively eliminates the SARS-CoV-2 virus and activates thymus immune function to exert antiviral effects[6]. In light of our previous investigations[6], we have observed that the active phosphorylated form of FNC, known as FNC-TP, exhibits significant enrichment in thymus tissues of both rats and rhesus monkeys, thereby playing a crucial immunoprotective role against SARS-CoV-2. Consequently, for this study on nucleotide phosphorylation metabolism in thymus cells, rats and rhesus monkeys were selected as the preferred experimental animal models due to their frequent utilization in research about the thymus and other immune-related studies. To elucidate the activation process of FNC in thymus cells and immune cells activation, particularly T cell, this study integrated tissue distribution, single-cell transcriptomics, and proteomics of the rat and SARS-CoV-2 rhesus monkey thymus to investigate alterations of the key metabolic enzymes associated with NAs phosphorylation activation process in thymus cells. The findings suggested that cytidine analogues such as FNC possess potential therapeutic advantages compared with other types of NAs following viral infection of T cells with a robust phosphorylation capacity. Furthermore, it is crucial to evaluate the expression level of NAs phosphorylation kinases during antiviral drug design, as the phosphorylation activation ability of NAs represents an important factor for consideration.

2. Materials and methods

2.1. Chemicals and reagents

FNC purchased from MedChemExpress (MCE, Shanghai, China). LC−MS-grade acetonitrile and methanol and HPLC-grade formic acid and ammonium bicarbonate were purchased from Fisher Scientific (New Jersey, USA). Iodoacetamide (IAA) and dithiothreitol (DTT) were purchased from Sigma (St. Louis, MO, USA), and sequencing-grade trypsin was purchased from Promega (Madison, WI, USA). Ultrapure water was prepared using a Milli-Q purification system (MA, USA). Ammonium hydroxide (LC/MS), ammonium acetate (LC/MS) and formic acid (LC/MS) were purchased from Sigma−Aldrich (St. Louis, MO, USA). 2-Propanol (Optima, LC/MS) were purchased from Fisher-Scientific (Loughborough, UK). HPLC-grade water was prepared using a Milli-Q Nanopure purification system (Billerica, MA, USA).

2.2. Ethics statement

The rat care and experimental procedures were reviewed and approved by the Institutional Animal Care and Use Committee of the Chinese Academy of Medical Sciences & Peking Union Medical College (approval No. 00003537). All procedures were carried out following the approved guidelines.

The rhesus monkey (RMs) experiments received approval from the Institutional Animal Care and Use Committee at the Institute of Medical Biology, Chinese Academy of Medical Science (Ethics number: DWSP202006001)[6]. The viral-infected animal experiment took place in the ABSL-4 Unit within the Kunming National High-level Biosafety Primate Research Center located in Kunming, China.

2.3. Animal experiments and drug administration

Male SD rats obtained from Beijing Vital River Laboratory Animal Technology Co., Ltd. were housed in a pathogen-free

environment, maintained at a temperature of 22 ± 2 °C and humidity ranging from 40% to 70%. They had *ad libitum* access to food and autoclaved water. After a two-week acclimation period, the animals were randomly divided into three groups: control group (n = 5), single-dosed FNC group (n = 5, 5 mg/kg, i.g.), and multiple-dosed FNC group (n = 5, 5 mg/kg, i.g. for five consecutive days). Two hours after FNC administration, euthanasia was performed on five rats from each group for sample collection. Tissues including thymus, spleen, liver, testis, kidney, and lung were collected and washed with cold normal saline solution (0.9% *w*/*v*) before being stored at −80 °C for tissue distribution analysis. Besides that, the fresh thymus tissues collected from both the multiple-dosed FNC group (n = 5, 5 mg/kg, 5 days, i.g.) and control group (without FNC administration) were subjected to single cell transcriptomic and proteomic studies, which were conducted 2 h after the final FNC administration.

The rhesus monkeys experiment followed the same methodology as described in the earlier publication. Briefly, a total of 8 healthy RMs (4 males and 4 females) aged between 3 and 4 years were utilized. All the RMs were intratracheally administered with SARS-CoV-2 at a concentration of 106 pfu/mL (0.5 mL) and intranasally inoculated with the same virus at the same concentration (0.5 mL). FNC treatment (0.07 mg/kg, qd, orally) along with vehicle administration was initiated 12 h after viral inoculation and continued for 7 days in both experimental and control groups respectively. The euthanized RMs underwent organ retrieval on day 8 for single-cell sequencing, then storage at −80 °C for proteomics study.

2.4. Cell culture

Human T lymphocyte leukemia cell Jurkat E6 was from the BeNa Culture Collection (#BNCC338675) and cultured in the RPMI-1640 medium (Invitrogen) supplemented with 10% fetal calf serum (FBS, Invitrogen), penicillin (100 U/mL) and streptomycin (100 μg/mL) (Invitrogen) at 37 °C and 5% CO_2. The cell experiment was divided into a control group (without FNC), an FNC administration group, and an FNC with nucleotide phosphorylated metabolic enzyme inhibitor administration group, respectively. In the day before FNC and inhibitors treatment, 5×10^6 cells were seeded into 100 mm dishes and activated with anti-CD3 antibody (100 ng/mL, Biolegend#317302) and anti-CD28 antibody (100 ng/mL, Biolegend# 302902) for 24 h. The inhibitors of each metabolite enzymes, including DI-82 as Dck inhibitor (100 nmol/L), EDTA as Cmpk1 inhibitor (10 mmol/L), and stauprimide as Nme2 inhibitor (10 μmol/L), were administrated for 6 h before FNC (10 μmol/L) treatment. After 24 h, the cell samples were collected in methanol and H_2O (80:20, *v*/*v*) and stored under −80 °C overnight. The cells were disrupted using a cell disruptor, and the resulting supernatant was subjected to centrifugation for subsequent analysis. Subsequently, the cell supernatant was dried with nitrogen, reconstituted in a 100 μL solution of acetonitrile/methanol (75:25, *v*/*v*) containing an internal standard (Phenylalanine-d_8), and then centrifuged at 4 °C for 15 min at a speed of 13,000 revolutions per minute. The resulting mixture was transferred to a liquid phase flask and stored at −80 °C for LC−MS/MS analysis.

2.5. Tissue distribution study

Tissue samples were weighed and homogenized with a 2-fold volume of 0.9% normal saline containing phosphatase inhibitor on ice, followed by ultrasonic extraction for 5 min in an ice bath. Then, 200 μL of plasma or tissue homogenate was transferred to a 1.5 mL Eppendorf tube and mixed with 600 μL of methanol solution containing internal standards. The sample was vortexed for 5 min, kept at 4 °C for 15 min, and then centrifuged at 13,000 rpm for 10 min (4 °C). After removing protein precipitation, the supernatant was transferred to another eppendorf tube and dried under gentle nitrogen stream. The residue was re-dissolved in acetonitrile/methanol (75:25 *v*/*v*) solution (100 μL) for LC−MS/MS analysis. We conducted quantitative analysis of FNC, FNC-MP, FNC-DP, and FNC-TP in rat tissues based on the matrix standard curves of each tissue, including thymus, spleen, liver, testis, kidney, and lung, respectively. Specifically, the FNC-MP and FNC-DP were quantitatively analyzed using the standard curves established for FNC-TP. The standard curves were presented in Supporting Information Table S1 with correlation coefficients (R2) exceeding 0.98. The accuracy and precision of LQC, MQC, and HQC samples meet the quantitative analysis requirements.

2.6. The LC−MS/MS analysis method

LC−MS/MS analysis was applied for the tissue distribution study of FNC and its active phosphorylated metabolites, and nucleotides/deoxynucleotides analysis of human T lymphocyte leukemia cells. The LC−MS/MS analysis was performed on an HPLC system (1290 series, Agilent Technologies) coupled to a triple quadrupole mass spectrometer (Agilent 6470 QQQ). The chromatographic separation was carried out on a Waters ACQUITY UPLC BEH Amide column (2.1 mm×150 mm, 1.7 μm). Mobile phase A was comprised 10 mmol/L ammonium acetate in water containing 0.5% ammonium hydroxide. Mobile phase B was comprised of acetonitrile/water (90:10, *v*/*v*) containing 10 mmol/L ammonium acetate and 0.5% ammonium hydroxide. A gradient elution was employed using the following program: 0−3 min, 100%−65% B; 3−7 min, 65%−60% B; 7−8 min, 60%−56% B. The flow rate was set at 0.3 mL/min, the column oven temperature at 30 °C, and an injection volume of 5 μL. The autosampler was set at 4 °C. AJS ESI source conditions were set as follows: sheath gas temperature, 250 °C; drying gas temperature, 300 °C; sheath gas flow rate, 11 L/min; drying gas flow rate, 5 L/min; capillary voltage, 3500 V; nozzle voltage, 500 V and nebulizer pressure, 45 psi. Multiple reaction monitoring (MRM) mode was performed using the characteristic precursor to product ion transitions as shown in the Supporting Information Tables S2 and S3, including FNC and its active phosphorylated metabolites, and nucleotides/deoxynucleotides.

2.7. Single-cell transcriptome analysis

Single-cell transcriptomics involves high-throughput sequencing of mRNA at the individual cell level, allowing for the exploration of heterogeneity within complex cell populations and avoiding the masking of gene expression signals by population averaging. As one of the leading platforms for single-cell transcriptomic sequencing, the 10× Genomics system, which enables large-scale analysis and finds extensive applications in studying cellular heterogeneity, immune profiling, and constructing cellular atlases, was applied for the exploration of FNC on nucleotide metabolism in various immune cells of the thymus. The cell viability was greater than 80% for quality inspection and counting of single-cell suspensions from rat and rhesus monkey thymus samples.

Subsequently, the qualified cells undergo washing and resuspension to achieve 700−1200 cells/μL for 10× Genomics analysis. Single-cell transcriptome analysis was conducted using the Illumina NovaSeq 6000 sequencing platform, with a PE150 sequencing mode.

2.8. Sample preparation for proteomic analysis

The samples from each group were prepared for LC−MS/MS analysis using EasyPep™ Mini MS Sample Prep Kit (Thermo Scientific, Waltham, MA, USA). Briefly, 100 μg/protein thymus tissue samples of rat (multiple-dosed FNC group (n = 5, 5 mg/kg, 5 days, i.g.) and control group (without FNC administration)) and rhesus monkey (FNC treatment group and SARS-CoV-2 infection group) were transferred into a new tube and adjusted to 100 μL general lysis buffer. Afterward, incubate the sample at 95 °C using a heat block for 10 min to reduce and alkylate the protein samples, 10% Trypsin/Lys-C mix was added to digest proteins at 37 °C for 2 h. Digestion was stopped by acidification and desalted using a peptide clean-up column.

2.9. Online nanoflow proteomics analysis

The protein samples (100 μg each) were dissolved in 80 μL of a solution containing 0.1% formic acid and 2% acetonitrile, and then subjected to analysis using the UHPLC-trapped ion mobility spectrometry coupled with tandem mass spectrometry (UHPLC−TIMS-TOF-MS) system from Bruker Technologies. The peptides (injected volume: 3 μL) were separated on a C18 reverse-phase capillary column (75 μm × 25 cm, Thermo Scientific, PepMap). Chromatographic separation was achieved by employing a continuous gradient of acetonitrile with 0.1% formic acid as mobile phase A and acetonitrile containing 0.1% formic acid as mobile phase B. The following program was run at 0.3 μL/min: 0−75 min, 2%−22% B; 75−80 min, 22%−37% B; 80−85 min, 37%−80% B; 85−90 min, 80% B.

The MS scan was conducted at a resolution of 60,000 with a mass range of m/z 100 to 1700 in positive mode. The parallel accumulation-serial fragmentation (PASEF) ramps were set to 10, resulting in a total cycle time of 1.17 s. The range of $1/k_0$ values was adjusted to be between 0.6 and 1.6 V s/cm^2, corresponding to collision energies ranging from 20 to 59 V. MS/MS analysis was performed on the most abundant intense signal exhibiting charge states from 0 to +5. Dynamic exclusion parameters were set at an interval of 0.5 min with a mass window tolerance of ±15 ppm.

2.10. Data processing for proteomics

The raw data files (*.d) were directly imported into PEAKS Studio (Bioinformatics Solutions, Inc.) for qualitative and quantitative analysis of the proteins. Both precursor mass tolerance and MS/MS tolerance were set to 15 ppm and 0.02 Da, respectively. Searches were performed with complete tryptic digestion, allowing a maximum of 2 missed cleavages. A false discovery rate (FDR) threshold of 1% was applied at both peptide and protein levels, and data processing utilized the standard legacy Peptide-Prophet scoring system. The PEAKS software employed a reverse decoy database by reversing the protein sequences from the target database. Relative protein abundance ratios were calculated, followed by permutation tests for statistical significance assessment. Proteins exhibiting P-values <0.05 and significant fold changes (>1.3 for up-regulated proteins and <0.769 for down-regulated proteins) were considered as differentially expressed.

2.11. Parallel reaction monitoring (PRM) proteomics

The PRM peptide screening was conducted using Skyline software (version 20.1.0.76). For each differentially expressed protein, unique peptides with high signal-to-noise ratios were selected for screening from the rat thymus tissue sample database. These selected unique peptides were subsequently subjected to PRM experiments, employing the same chromatographic separation as the online nanoflow proteomics analysis. The MS1 resolution was set at 40,000 and the collision energy was adjusted in "Rolling Collision Energy" mode. Charge state screening was limited to precursors with a +2 to +4 charge state range. The MS/MS scan range spanned from m/z 350−1500 with a resolution of 20,000, while dynamic exclusion time was set at 15 s. Mass spectrometry data files were imported into Skyline software for data integration and analysis purposes, including spectral library creation, manual inspection of fragment ions, as well as selection and quantification of target proteins using unique peptides. The three strongest daughter ions were selected for quantitative analysis of unique peptides based on their peak area data.

2.12. Gene set enrichment analysis (GSEA)

The COVID-19 monkey thymic cell sample from the untreated group was compared to the FNC-treated sample in our previous study. We analyzed the differentially expressed genes (DEGs) of different cell clusters using the R 4.3.1 "Seurat" (4.4.0) package based on the previous single-cell RNA sequence data. To identify pathways associated with untreated and FNC-treated samples, we performed Gene Set Enrichment Analysis (GSEA) using the "ClusterProfiler" (4.8.3) package, considering a statistically significant threshold of P-value <0.05 and $P_{adjust} < 0.5$.

2.13. Statistical analysis

Statistical analyses were performed using the SPSS software program (version 19.0, Chicago, IL, USA). All data represent biological replicates (n) and were expressed as mean ± SEM. One-way analysis of variance (ANOVA) with the post hoc test followed by Student's t-test was performed. P values less than 0.05 were considered to be statistically significant.

2.14. Data availability

The raw single-cell sequencing data (.fastq) were uploaded to the genome sequence archive (GSA) public database, with the dataset number: CRA015371. The mass spectrometry proteomics data have been deposited to the ProteomeXchange Consortium *via* the PRIDE[15] partner repository with the dataset identifiers PXD050620 and PXD050624.

3. Results

3.1. Distribution of FNC and its phosphorylated metabolites in rat tissues under single and multiple doses

As shown in Fig. 1A and B, FNC and its active phosphorylated metabolites in rats were identified by our developed UHPLC−MS/MS

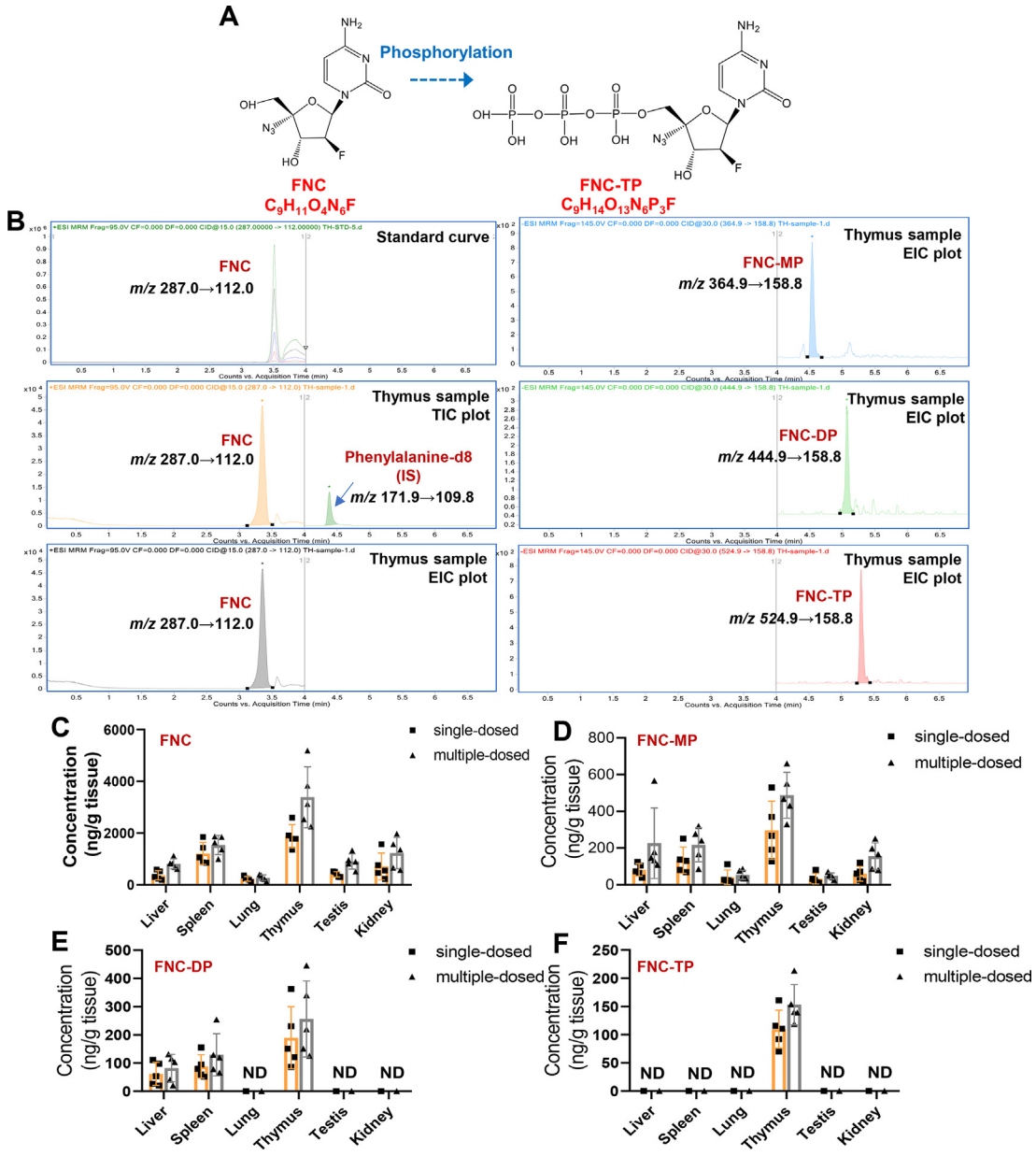

Figure 1 The distribution of FNC and its metabolites in rat thymus. (A) Structure of FNC and its triphosphorylated metabolites; (B) the MRM chromatograms of FNC and its metabolites in rat thymus; (C) FNC distribution in rat tissues with single and multiple-dosing; (D) FNC-MP distribution in rat tissues with single and multiple-dosing; (E) FNC-DP distribution in rat tissues with single and multiple-dosing; (F) FNC-TP distribution in rat tissues with single and multiple-dosing.

method (Table S2). FNC could be absorbed into the tissues and metabolized to mono-phosphorylated metabolite (FNC-MP), di-phosphorylated metabolite (FNC-DP) and tri-phosphorylated metabolite (FNC-TP) *in vivo*. The FNC prototype was exposed in the thymus, spleen, liver, testis, lung, and kidney, respectively. The results demonstrated that FNC exhibited predominant enrichment in immune-related tissues, including the thymus and spleen. Following a single dose administration of 5 mg/kg *via* oral gavage, the exposure concentrations were determined to be 1910 ng/g in the thymus and 1182 ng/g in the spleen after a 2-h administration. In the case of multi-dose (5 days) exposure, the concentration increased to 3252 ng/g in the thymus and 1578 ng/g in the spleen, respectively (Fig. 1C). FNC-MP, which serves as a crucial intermediate product during FNC's triphosphorylation process within cells, was primarily enriched in the thymus, spleen, liver, and kidney. After a 2-h administration of 5 mg/kg FNC *via* oral gavage, respective exposure concentrations of FNC-MP were measured at 293 ng/g in the thymus, 110 ng/g in the spleen, 76 ng/g in the liver, and 59 ng/g in the kidney. Upon multiple doses (5 days), these concentrations rose to values of approximately 482 ng/g for thymus tissue, 201 ng/g for spleen tissue, 206 ng/g for liver tissue, and 156 ng/g for kidney tissue (Fig. 1D). FNC-DP could be detected in thymus, spleen, and liver tissue. The highest exposure level of FNC-DP among tissues was quantified in thymus tissue, and the average exposure concentration after single and multiple intragastric administration was 190 ng/g and 256 ng/g, respectively (Fig. 1E). Notably, FNC-TP, the active metabolite of FNC, was exclusively detected within the thymus tissue. The exposure concentration of FNC-TP in the thymus was 108 ng/g following a single

dose administration, and 149 ng/g under multiple doses (5 days), which were below the detection limits in other tissues (Fig. 1F). In summary, FNC along with its phosphorylated metabolites demonstrated predominant enrichment within immune-related tissues, such as the thymus and spleen. Furthermore, FNC-TP was only detected in the thymus. In this study, the tissue distribution of rats with single and multiple dosed administration of FNC was evaluated, and the exposure and accumulation level of FNC and its active metabolites in each tissue were obtained. The results showed that the thymus was the main tissue exposed to FNC and its active metabolites, and there was no significant difference in exposure level between multiple-dosed administration and single-dosed administration, indicating that there was no tissue accumulation after multiple administration of FNC. These results provided a reference for the evaluation of *in vivo* exposure to the clinical drug administration of FNC.

3.2. *Thymic immune cells possess a robust phosphorylation capacity for FNC*

The transportation of NAs drugs into cells relies on transmembrane transport proteins, specifically the nucleoside transporter family, as depicted in Fig. 2A. Subsequently, these drugs undergo a series of metabolic processes including monophosphorylation, diphosphorylation, and triphosphorylation to attain their active forms. The cytidine analogue drug FNC primarily undergoes phosphorylation in cells, firstly generating the monophosphorylated metabolite (FNC-MP) *via* Deoxycytidine kinase (Dck), followed by conversion to the diphosphorylated metabolite (FNC-DP) through UMP-CMP kinase (Cmpk1), and ultimately leading to the formation of the triphosphorylated metabolite (FNC-TP) *via* Adenylate kinase (Ak1−9) and Nucleoside diphosphate kinase (Nme1−7). To understand the expression of these key genes in various cell types within the thymus tissue, which is the critical pharmacological target tissue for FNC, we conducted single-cell transcriptome analysis of rat and rhesus monkey thymus tissues. By grouping based on marker genes, a total of seven cell types were classified in rat thymus tissue: CD4+ T cells, CD8+ T cells, DP cells (double positive, CD4+, CD8+), DN cells (double negative, CD4−, CD8−), B cells, macrophage cells and Treg cells, respectively (Supporting Information Table S4 and Fig. S1). Key genes related to FNC transport and phosphorylation were identified from each cell type present in rat thymus tissue (Fig. 2B). The key genes responsible for cytidine analogue monophosphorylation, Dck, and diphosphorylation, Cmpk1, were predominantly expressed in CD4+ T cells, CD8+ T cells, and DP cells. Parallelly, key genes involved in FNC triphosphorylation including Nme1 and Nme2, exhibited high expression levels specifically in CD4+ T cells, CD8+ T cells, and DP cells. The nucleotide transport protein such as Slc29a1 exhibited predominant expression in CD4+ T cells and DP cells, respectively. These findings suggested that the enzymes involved in FNC phosphorylation process were highly expressed primarily in major subsets of thymic lymphocytes, including CD4+ T cells, CD8+ T cells, and DP cells.

Comparison of the total expression levels of nucleoside monophosphate kinases, such as adenosine kinase (Adk), deoxycytidine kinase (Dck), deoxyguanosine kinase (Dguok), thymidine kinase (Tk), uridine-cytidine kinase (Uck) and others (shown in Fig. 2C and D), Dck for phosphorylation of cytidine analogues such as FNC exhibits the highest expression level both in rat and rhesus monkey thymus cells. Similarly, among nucleoside diphosphate kinases, including deoxythymidylate kinase (Dtymk), UMP-CMP kinase (Cmpk), and guanylate kinase (Guk), Cmpk1 for phosphorylation of cytidine analogues exhibit the highest expression level in rat and rhesus monkey thymus cells. Among nucleoside triphosphate kinases, including adenylate kinase (Ak), nucleoside diphosphate kinase (Nme), and pyruvate kinase, Nme2 exhibit relatively high expression levels in rat and rhesus monkey thymus cell types, respectively. Simultaneously, Dck, Cmpk1, and Nme2 exhibit the highest expression level in major thymic cell types such as DP cells, CD4+ T cells, CD8+ T cells, and DN cells in rat and rhesus monkey thymus cells (Fig. 2E and F). Furthermore, Human T lymphocyte leukemia cell was incubated with FNC in the presence of specific inhibitors targeting Dck, Cmpk1, and Nme2. The results demonstrated that inhibition of Dck significantly attenuated the metabolism of FNC to FNC-MP, highlighting the substantial impact of nucleotide phosphorylated kinases such as Dck on the conversion of FNC into its active phosphorylated form (Supporting Information Fig. S2). The above single-cell transcriptome data indicated that thymic immune cells possess a robust metabolic capacity for cytidine analogues such as FNC. Key enzymes involved in phosphorylation metabolism, such as Dck, Cmpk1, and Nme2, were highly expressed in thymus T cells, including DP cells, CD4+ T cells, CD8+ T cells, and DN cells of the rat and rhesus monkey, respectively. Metabolic enzymes involved in nucleotide phosphorylation metabolism were found to be highly expressed across multiple subtypes of T cells, suggesting that the metabolism of FNC primarily occurs within these cells. Considering the changes in proportion and function observed in T cells, it is possible that the antiviral activity of FNC on other immune cell types, such as NK cells, might be directly regulated by T cells[16]. Within T cells, FNC undergoes metabolic conversion into FNC-TP, thereby enhancing the immune response and potentially influencing the functional behavior of NK and other immune cell types.

3.3. *FNC activated the nucleotide and NAs key metabolic enzymes in rat thymus cells, especially in CD4+T cells*

During the phosphorylation process of nucleoside analogs, various metabolic enzymes in the cell can exert influence on their phosphorylation. In Supporting Information Table S5, we have compiled a summary of the types of metabolic enzymes and their corresponding gene lists that may participate in FNC metabolism. These included nucleoside transport proteins and kinases involved in nucleoside analog transportation and phosphorylation processes, as well as deaminases, phosphoribosyl transferases, and phosphatases. Fig. 3A and B illustrated the categories involved in nucleoside analogs transportation and phosphorylation processes and presented the respective number of genes associated with these enzymes along with their specific metabolic pathways and sites of action on FNC. We identified seven types of cells in the rat thymus through single-cell transcriptome analysis: CD4+ T cells, CD8+ T cells, DP cells, DN cells, B cells, Macrophage cells, and Treg cells (Fig. 3D). These cell types had different proportions in the thymus, with DP cells being the most abundant (51%), followed by CD4+ T cells (35%) and CD8+ T cells (9%) (Fig. 3C). Analyzing the changes in metabolic enzymes in each type of thymic cell before and after FNC administration can elucidate the activation status of nucleotide and nucleoside metabolism system induced by FNC. The findings indicated that significant changes (*t*-test $P < 0.05$) occur in the metabolic enzymes of nucleotides and nucleoside in CD4+ T cells from rat thymus (Fig. 3E). Following FNC administration, there was a significant increase in the expression levels of monophosphorylation kinases Dguok and

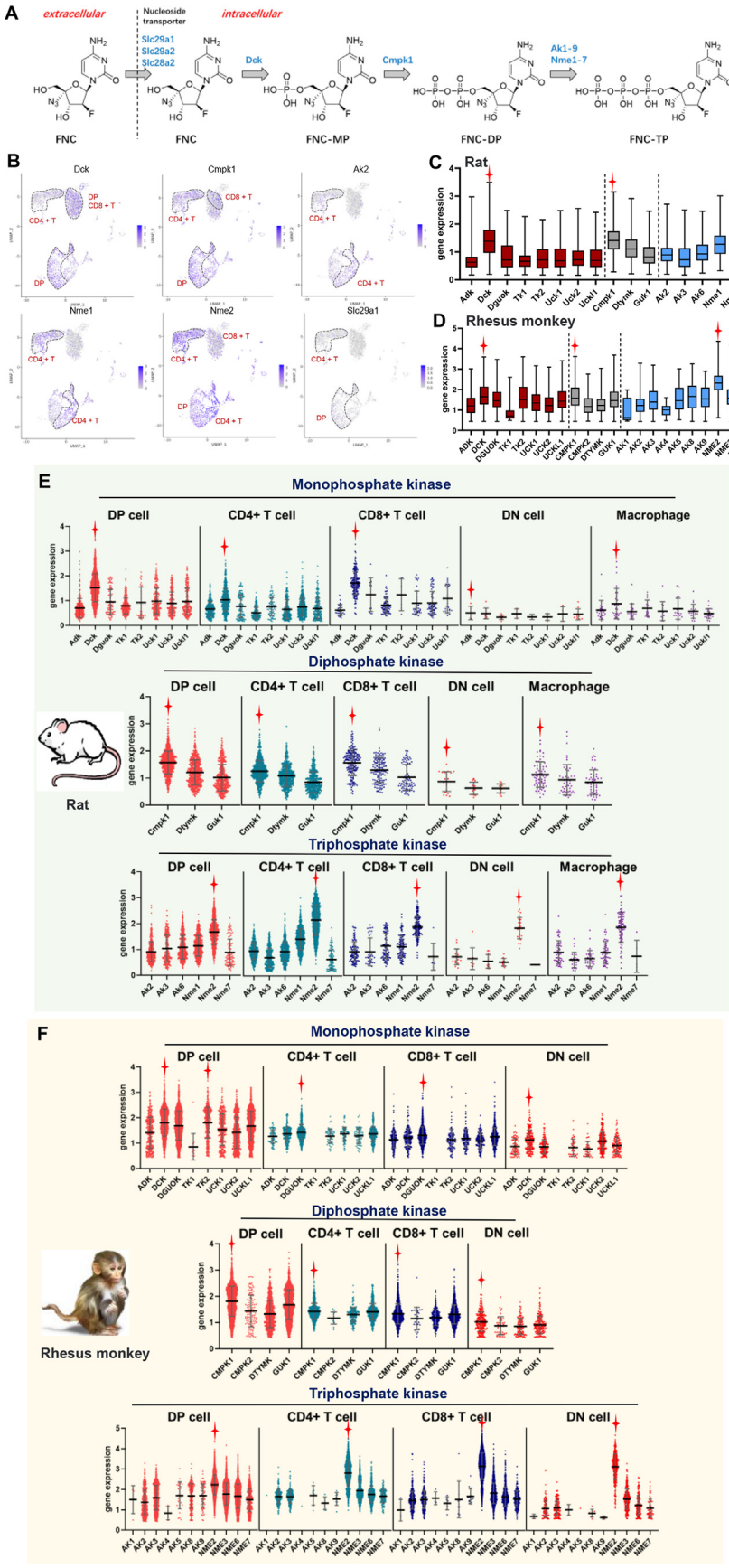

Figure 2 The expression of FNC phosphorylation-related metabolic enzymes in different subtypes of thymus cells. (A) The key proteins involved in the transport and metabolism processes of FNC; (B) gene expression of key proteins involved in FNC transport and phosphorylation in

Tk1, as well as diphosphorylation kinase Dtymk. Additionally, triphosphorylation kinases Nme1, Nme2, and Pkm showed a substantial increase in expression levels. Conversely, adenosine deaminase, Ada and various types of phosphohydrolases such as Nt5c2 from the 5′-nucleotidase family and Entpd5 from the ectonucleoside triphosphate diphosphohydrolase family exhibit a notable decrease in expression levels. These results suggested that FNC promoted phosphorylation processes of nucleotides and nucleosides in CD4+ T cells of the thymus tissue. In other major categories of thymic cells including CD8+ T cells, DP cells, DN cells, and macrophages, fewer changes in metabolic enzymes were observed compared to CD4+ T cells, including various types of phosphorylation kinases and phosphohydrolases. The details are displayed in Fig. 3F.

3.4. Proteomics revealed the effect of FNC on the expression of nucleotide metabolic enzymes in the thymus tissue

We further conducted proteomic studies on thymus tissues of rats and rhesus monkeys to explore the regulatory role of FNC in the metabolism of nucleotides and nucleoside analogs within thymocytes (Fig. 4A and E). The thymus tissues of rats were divided into a multiple-dosed FNC group ($n = 5$, 5 mg/kg, 5 days, i.g.) and a control group (without FNC administration). After protein lysis and enzymatic digestion of the thymus tissues, proteomics analysis was conducted. A total of 34 proteins were identified in the database through comparison with the nucleotide and nucleoside analog metabolism enzymes database. PCA analysis was shown in Fig. 4B. Proteins showing a fold change >1.3 and *t*-test $P < 0.05$ were selected as differentially expressed proteins between groups. A total of 10 differentially expressed proteins were identified, as shown in the heatmap analysis (Fig. 4C) and volcano plot (Fig. 4D). In rat thymus tissues, significant upregulation was observed for monophosphorylated kinases Dguok and Tk1 after FNC treatment, triphosphorylated kinase Pkm, Ak1 and Nme4 also showed significant upregulation. On the other hand, deaminase Ada, phosphoribosyl transferase Aprt, and Nt5dc1, Nt5c2, Nt5c3b of 5′-nucleotidase family proteins exhibited significant downregulation. Consistent findings were observed in the rat single-cell transcriptome and thymus proteome, indicating significant differences in proteins with or without FNC administration. Notably, monophosphorylated kinases Dguok and Tk1, as well as triphosphorylated kinase Pkm, exhibited consistent changes. Moreover, Nucleoside diphosphate kinase family (Nme) proteins—Nme1 and Nme2—showed high expression levels after FNC administration according to single-cell transcriptome data; however, these proteins were not identified in the thymus proteomics study. Conversely, Nme4 displayed increased expression following FNC administration. In conclusion, both the rat single-cell transcriptome and proteomics data provide evidence of FNC activation on nucleotide phosphorylation metabolism. The thymus tissues of rhesus monkeys were divided into a control group (SARS-CoV-2 infection) and an FNC treatment group. After protein lysis and enzymatic digestion of the thymus tissues, proteomics analysis was conducted. A total of 18 proteins were identified in the database through comparison with the nucleotide and nucleoside analog metabolism enzymes database. PCA analysis was shown in Fig. 4F, and proteins showing fold change >1.3 and *t*-test $P < 0.05$ were selected as differentially expressed between groups. A total of 9 differential proteins identified through this screening process, as depicted in the heatmap analysis presented in Fig. 4G and volcano plot analysis presented in Fig. 4H. In the thymus tissues of rhesus monkeys, significant upregulation was observed for phosphorylating kinases Ak2, Ak3, and Nme2 after FNC administration; while adenosine deaminase Ada, phosphoribosyl transferase Hprt1, Dnph1 as well as phosphohydrolases/nucleoside hydrolases Dut, Pnp, Dctpp1 showed significant downregulation. Based on the mentioned findings, it could be inferred that following FNC administration in thymus tissues of rats and rhesus monkeys, there was an upregulation in the expression levels of various types of phosphorylating kinases, while a downregulation was observed in the expression levels of deaminases and phosphohydrolases.

To further verify the activation of FNC on the metabolism of nucleotide phosphorylation in T cells. We established the LC−MS/MS method for 20 nucleotides/deoxynucleotides analysis, including NMP/dNMP, NDP/dNDP, and NTP/dNTP (Supporting Information Table S3 and Fig. S3). We compared the intracellular concentrations of nucleotide monophosphates, nucleotide diphosphates, and nucleotide triphosphates in Human T lymphocyte leukemia cells treated with or without FNC. The results demonstrated a significant increase ($P < 0.05$) in the abundance of UTP and GTP in FNC-treated cells. Additionally, the levels of ADP and GDP were significantly elevated ($P < 0.05$) upon FNC treatment in Human T lymphocyte leukemia cells. No substantial alterations were observed in Human T lymphocyte leukemia cells of nucleotide monophosphates treated with or without FNC (Supporting Information Fig. S4). The above results further proved that FNC could activate the phosphorylation metabolism of nucleotides/deoxynucleotides in T cells. The MRM chromatograms of all 20 nucleotides/deoxynucleotides in Human T lymphocyte leukemia cell were shown in Fig. S3, and the effect of FNC on the metabolism of each nucleotide/deoxynucleotide were shown in Fig. S4. Furthermore, we assessed the regulatory impact of FNC on nucleoside metabolism mediated by deaminase Ada and determined the substrates adenosine/2′-deoxyadenosine and metabolites inosine/2′-deoxyinosine catalyzed by Ada using an LC−MS/MS method. The results demonstrated a significant reduction in the levels of metabolic reaction products, namely inosine and 2′-deoxyinosine, within Human T lymphocyte leukemia cells following FNC administration (Supporting Information Fig. S5). This suggests that FNC may attenuate the enzymatic activity of deamination, aligning with the proteomics findings. These outcomes validate the single-cell transcriptome and proteome data by confirming that FNC enhances nucleotide phosphorylation metabolism in T cells through upregulation of nucleotide phosphokinase while downregulating phosphohydrolase and deaminase.

These results suggested that FNC could activate the nucleotide and nucleoside analogs phosphorylation metabolic system in thymocytes of rats and rhesus monkeys, by regulating the intracellular expression level of nucleotide phosphorylated kinases,

different types of immune cells in the thymus; (C) comparison of total expression of nucleotide phosphorylated kinases in rat thymus; (D) comparison of total expression of nucleotide phosphorylated kinases in rhesus monkey thymus; (E) gene expression levels of nucleotide metabolic enzymes in various types of rat thymic cells; (F) gene expression levels of nucleotide metabolic enzymes in various types of rhesus monkey thymic cells.

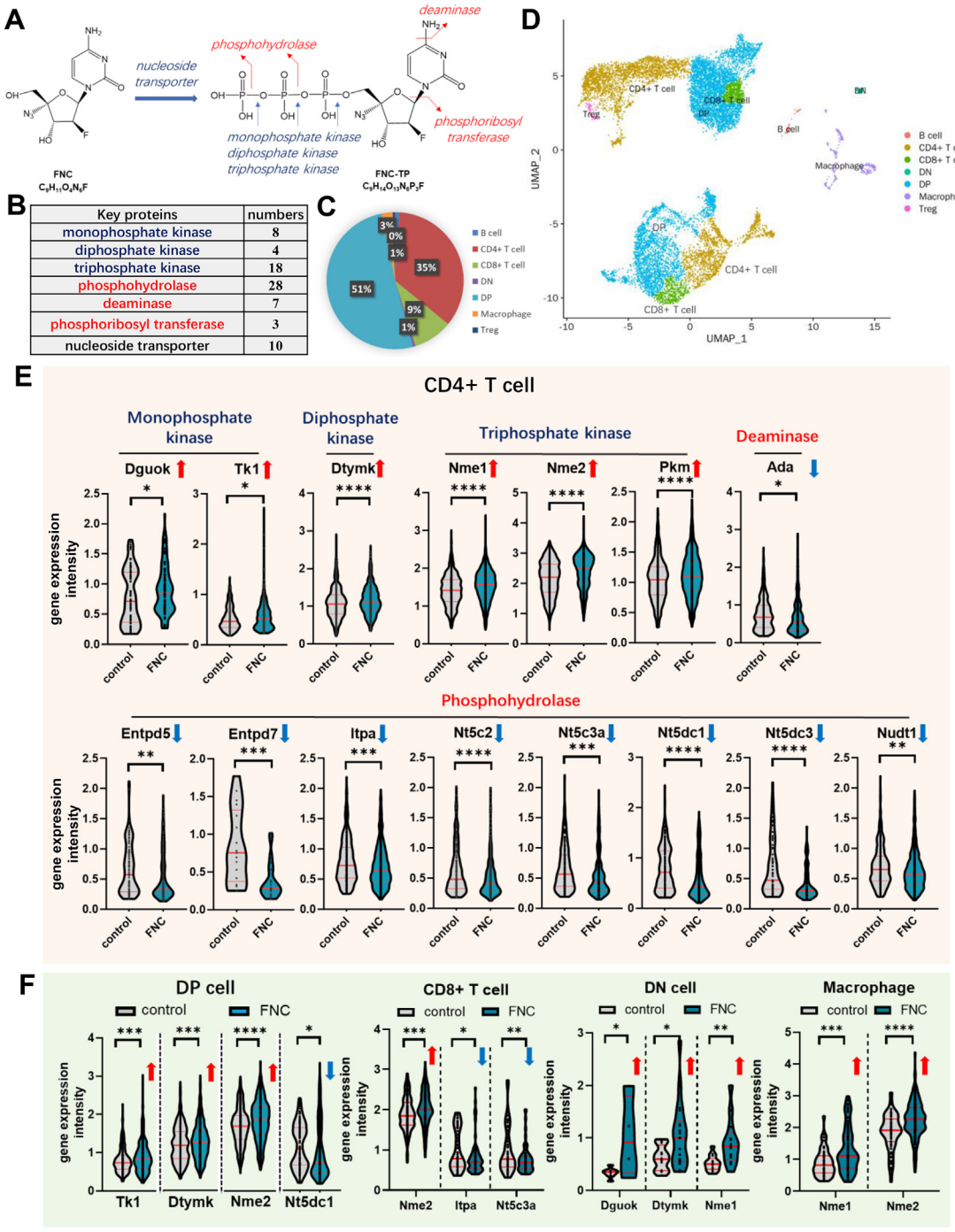

Figure 3 FNC activated the nucleotide and nucleoside analogues metabolism system in thymus cells. (A) Various types of nucleotide metabolic enzymes and their active sites; (B) number of nucleotide metabolism enzymes categorized by type; (C) the proportion of different types of thymus cells; (D) single-cell transcriptome analysis of various types of immune cells in the thymus; (E) the effect of FNC on nucleotide metabolism enzymes of CD4+ T cells in rat thymus; (F) the effect of FNC on nucleotide metabolism enzymes of other types of immune cells in rat thymus.

phosphohydrolases, and deaminases, thereby effectively exerting antiviral activity.

3.5. Parallel reaction monitoring proteomics verified the effect of FNC on nucleotide metabolic enzymes in the thymus tissue

Parallel reaction monitoring (PRM) proteomics is currently the mainstream method for targeted protein proteomics data acquisition. It selectively detects unique peptides or target peptides (such as post-translationally modified peptides), enabling targeted relative or absolute quantification of the target proteins/peptides. A targeted differential protein spectrum database was established specifically for rat thymus tissue, and Skyline software was utilized for PRM peptide screening (Fig. 5A). Mass spectrometry data files were imported into the Skyline software to enable data integration and analysis, which included the creation of spectral libraries, manual inspection of

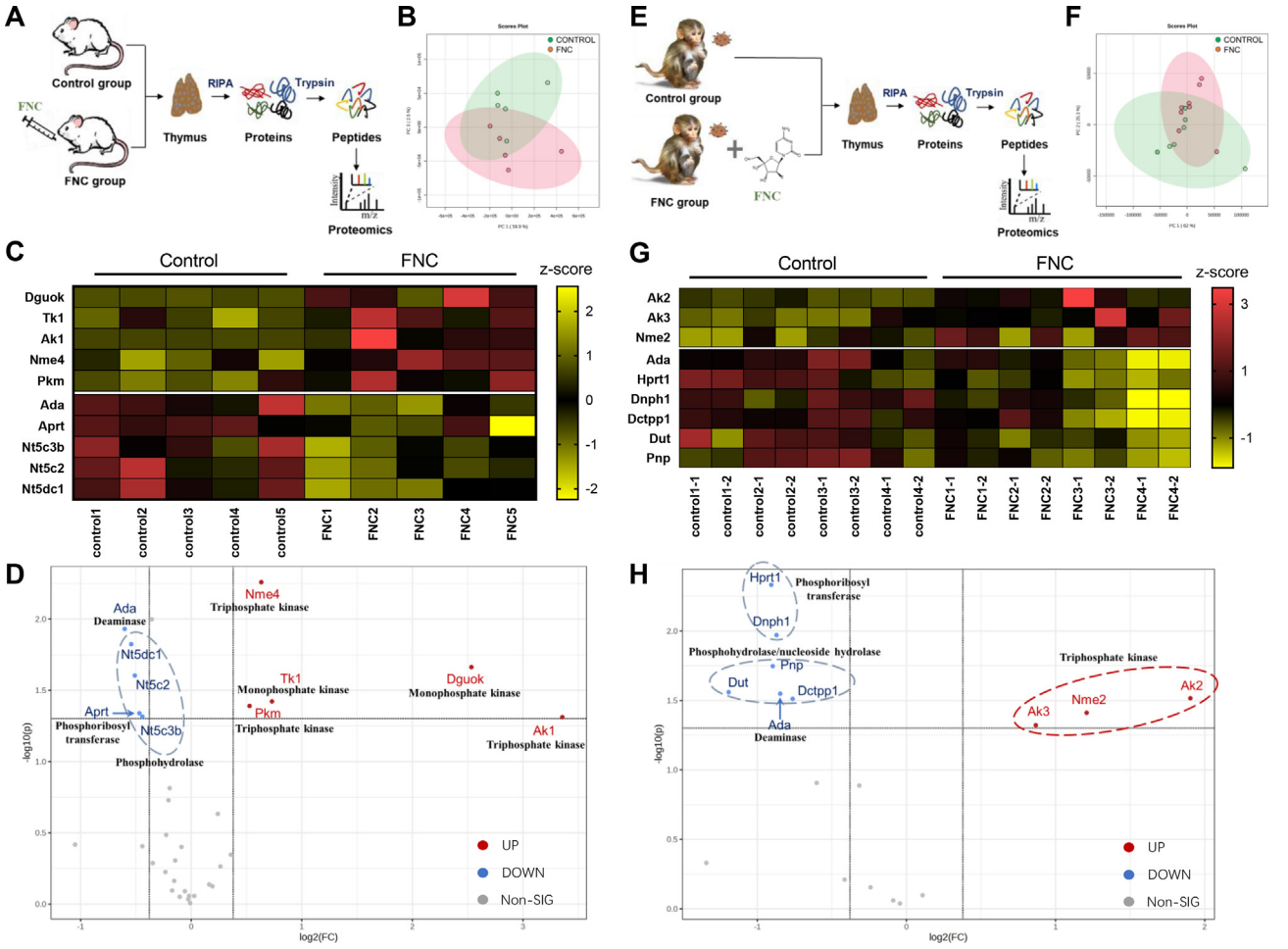

Figure 4 Proteomics of rats and rhesus monkey thymus tissue. (A) Proteomic experimental workflow of rat thymus; (B) PCA plot compared control group with FNC group in rat; (C) the heatmap of the differential proteins compared control group with FNC group in rat; (D) the volcano plot of the differential proteins compared control group with FNC group in rat; (E) proteomic experimental workflow of rhesus monkey thymus; (F) PCA plot compared control group with FNC group in rhesus monkey; (G) the heatmap of the differential proteins compared control group with FNC group in rhesus monkey; (H) the volcano plot of the differential proteins compared control group with FNC group in rhesus monkey.

fragment ions, as well as selection and quantification of target proteins using unique peptides. The daughter ions were selected for quantitative analysis of unique peptides based on their intensity data. The unique peptide total intensity was determined by utilizing the three daughter ions with the highest strength and stability in the unique peptide. The cumulative intensity of these three daughter ions was calculated to facilitate comparison between groups, while simultaneously mitigating potential fluctuations in peptide intensity resulting from systematic errors in mass spectrum response. We performed PRM analysis on key proteins identified in the thymus proteome of rats, including monophosphorylated kinase Dguok [unique peptide: R.LLQADTSVR.V], triphosphorylated kinase Ak1 [unique peptide: K.YGYTHLSTGDLLR.A], deaminase Ada [unique peptides: R.YSPHLLANSK.V and R.VGHGYHTIEDEALYNR.L], and phosphohydrolase Nt5dc2 [unique peptides: K.ITMLITSSHSDYCK.L and K.WGSYFIDSVSR.R], representatively (Fig. 5B−G). Specifically, Skyline software identified 1 unique peptide each for Dck and Ak1, as well as 2 unique peptides each for Ada and Nt5dc2, enabling inter-group comparison of protein expression levels. The optimized quantification results based on peak areas of characteristic peptide ions showed that the expression levels of monophosphorylated kinase Dguok and triphosphorylated kinase Ak1 significantly increased after FNC administration. Conversely, the expression levels of deaminase Ada and phosphohydrolase Nt5dc2 were significantly decreased, consistent with the findings from thymus proteomics. This validated the activating effect of FNC administration on the nucleotide phosphorylation metabolism system in rat thymic cells.

3.6. Functional analysis revealed that FNC activates thymus immune response to SARS-CoV-2 in rhesus monkey

The DEGs of different cell subtypes, which were re-analyzed from our previous study, were performed by GSEA analysis. In DP cells, the "response to virus", "innate immune response", and "immune response" pathways were significantly enriched and downregulated in the untreated sample ($P < 0.05$ and $P_{adjust} < 0.25$, Untreated *vs.* FNC-treated), which means FNC treatment upregulated these pathways in DP cells. The downregulated pathways in CD4+ T cells included "defense response to virus" and "immune response", while the upregulated pathway contains "Coronavirus disease-COVID-19" ($P < 0.05$ and $P_{adjust} < 0.25$, Untreated *vs.* FNC-treated). These illustrated FNC treatment attenuate the disease induced by COVID-19. The DEGs

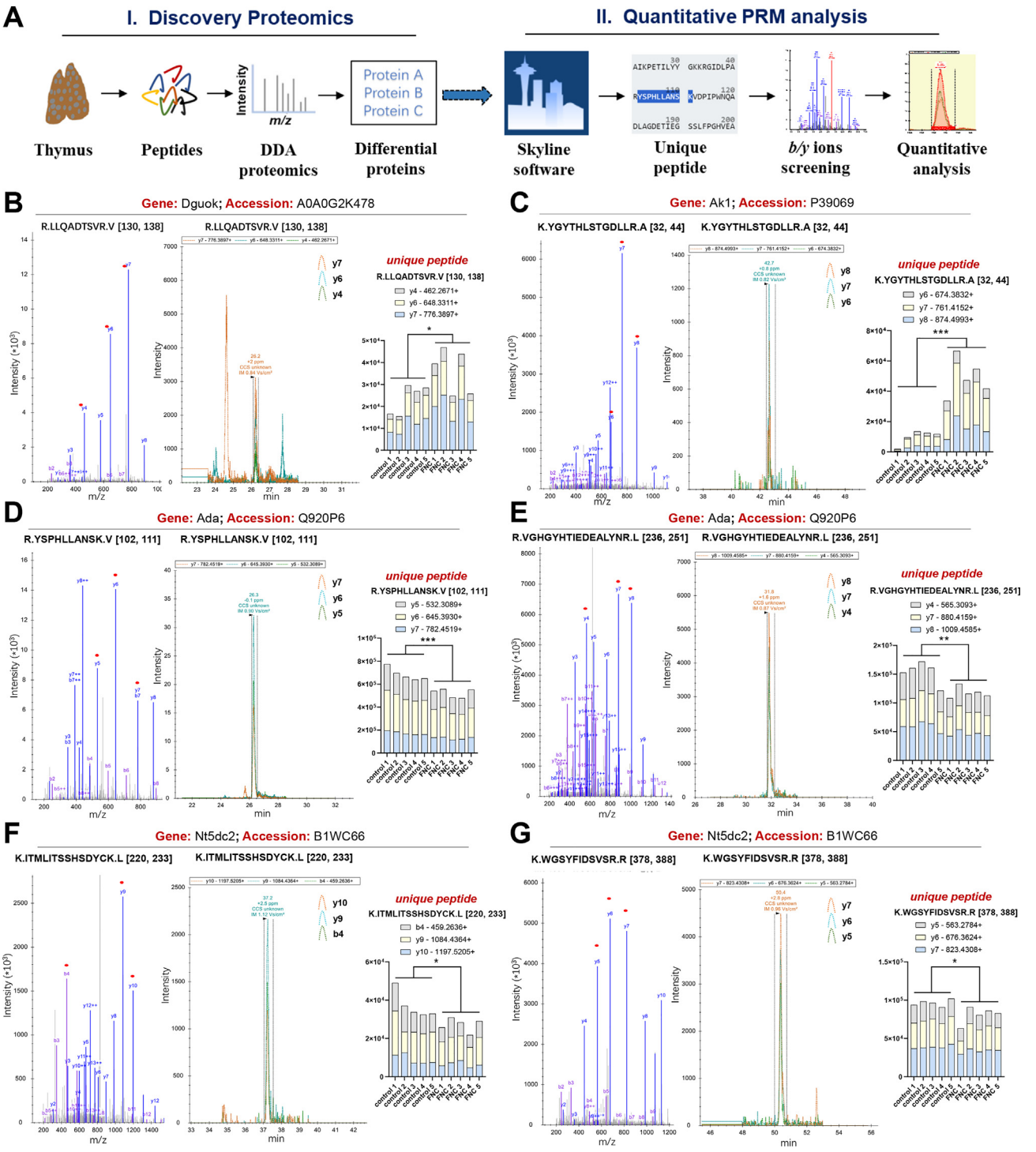

Figure 5 PRM verified the effects of FNC administration on nucleotide metabolic enzymes. (A) The workflow of PRM analysis; (B) PRM analysis on monophosphorylated kinase Dguok; (C) PRM analysis on triphosphorylated kinase Ak1; (D−E) PRM analysis on deaminase Ada; (F−G) PRM analysis on phosphohydrolase Nt5dc2.

in CD8+ T cells were enriched in the "defense response to virus" and "Coronavirus disease-COVID-19" pathway. Compared to the FNC-treated sample, the untreated sample had upregulated effect in the "Coronavirus disease-COVID-19" pathway and downregulated effect in the "defense response to virus" pathway ($P < 0.05$ and $P_{adjust} < 0.5$, 0.25, Untreated *vs.* FNC-treated). Although the P_{adjust} value in enrichment of the "Coronavirus disease-COVID-19" pathway in CD8+ T cell was greater than 0.25, the biological significance of this pathway was confirmed by the therapeutic effect in our previous study. The enriched pathways of NK T cells included "defense response to virus" and "innate immune response", which were both downregulated in untreated samples ($P < 0.05$ and $P_{adjust} < 0.25$, Untreated *vs.* FNC-treated). Thus, these enrichment results indicated that the

FNC treatment enhanced the defense response to SARS-CoV-2 infection and promoted the immune response of T cells in the thymus (Fig. 6).

Exploratively, we conducted a correlation analysis between key metabolic enzymes DCK, CMPK1, NME2 and the genes enriched in the 'defense response to virus' pathway within T cells of SARS-CoV-2-infected rhesus monkeys treated with FNC. However, as depicted in Supporting Information Fig. S6A, no significant correlations were observed between these crucial metabolic enzymes and the genes involved in the 'defense response to virus' pathway. Meanwhile, the protein−protein interaction networks (PPI) among these genes were analyzed using the STRING database (Fig. S6B). It was found that DCK, CMPK1, and NME2 interacted with antiviral functional proteins such as EIF2AK2, IFIT2, and IRF7 respectively. Subsequently, a correlation analysis was conducted between DCK, CMPK1, NME2 and EIF2AK2, IFIT2, and IRF7 in Fig. S6C. Additionally, the correlation between metabolic enzymes DCK, CMPK1, NME2, and genes enriched in the "immune response" pathway was investigated. In Fig. S6D, the triphosphorylation metabolic enzyme NME2 exhibited a correlation with GZMM, CCR7, and IL7R, which are associated with the process of antiviral immune response[17−19]. The positive correlations between NME2 and GZMM, CCR7, and IL7R have been individually analyzed in Fig. S6E. These correlation results indicated a positive association between the crucial metabolic

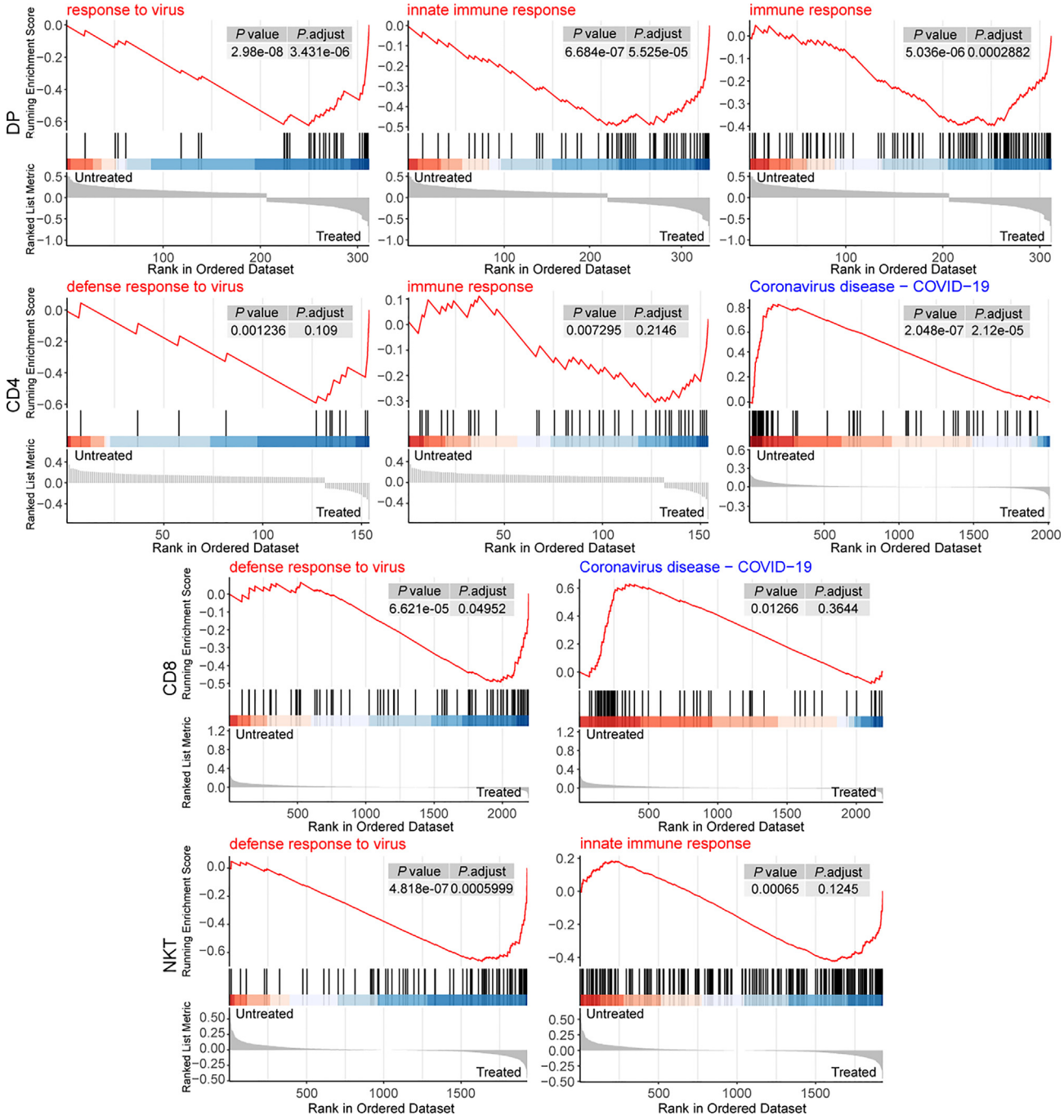

Figure 6 GSEA results of DEGs in DP, CD4, CD8, NKT cell subtypes of SARS-CoV-2 rhesus monkey thymus (Untreated *vs.* FNC-Treated).

enzymes DCK, CMPK1, NME2, and antiviral functional proteins that warrants further investigation.

4. Discussion

An immunocompetent and self-tolerant pool of naive T cells is formed in the thymus through the process of repertoire selection[20]. T cells that are potentially capable of responding to foreign antigens are positively selected in the thymic cortex and are further selected in the thymic medulla to help prevent self-reactivity during SARS-CoV-2 infection. At present, there is a lack of consideration of NAs activation on viral inhibition in thymus immune cells. FNC is a thymus-homing anti-SARS-CoV-2 drug effective in treating COVID-19 patients at low dose, and the active triphosphorylated metabolite (FNC-TP) was only detected in the thymus. It has been reported that SARS-CoV-2 is capable of infecting the thymus tissue in rhesus monkeys. The preferential elimination of the SARS-CoV-2 virus from the thymus tissue promotes enhanced immune response and systemic antiviral efficacy. FNC, as antiviral cytidine analogue drug, specifically targets the thymus tissue and exhibits a preferential reduction in viral load compared to the lung tissue in rhesus monkeys. However, the activation process of FNC in the thymus as its active form (FNC-TP) remains unclear. Therefore, this study explored the phosphorylation activation of FNC in thymus and the activation of immune cells.

This study conducted transcriptomic and proteomic analyses on rats and rhesus monkeys, revealing high expression levels of cytidine analogues phosphorylated kinases in various types of thymic T cells. NAs are a class of antiviral and anticancer drugs whose mechanism of action involves the interaction of their 5′-phosphorylated derivatives with essential enzymes such as DNA and RNA polymerases, ribonucleotide reductase and thymidylate synthase[21]. Following their entry into cells by specific nucleoside transporters, NAs are phosphorylated stepwise by nucleoside/nucleotide kinases to form their pharmacologically active metabolites. Nucleotides may be synthesized in the cells either de novo from small precursor molecules, or from simple metabolic pathways allowing the incorporation of already synthesized purines or pyrimidines to nucleotides—this is the salvage pathway[22]. The therapeutic activity of NAs depends largely on their efficient conversion to pharmacologically active phosphorylated forms through the salvage pathway of nucleotide synthesis. The salvage pathway enzymes TK, Dck and Dgk play a crucial role in activating therapeutically relevant NAs in first phosphorylation step. The last phosphorylation step of the NAs is mainly catalyzed by nucleoside diphosphate (NDP) kinases (Nme1−7) and adenylate kinases (Ak1−9), with similar efficiency observed for the second step. NDP kinases are housekeeping enzymes, responsible for the cellular equilibrium between nucleotides di- and triphosphate. In general, ATP serves as a donor of phosphate due to its high cellular concentration. As mentioned earlier, phosphorylations of NA drugs are necessary for their activation. On the contrary, their dephosphorylation by deaminase, phosphoribosyl transferase, as well as phosphohydrolases/nucleoside hydrolases may reduce their efficiency by increasing the relative concentrations of the inactive by-products compared to the active triphosphate counterparts[11,23,24]. Therefore, we have established a gene and protein database related to the intracellular transport and metabolism of nucleotides and nucleoside analogs. This includes nucleoside transporters, nucleotide monophosphorylating kinases, nucleotide diphosphorylating kinases, nucleotide triphosphorylating kinases, deaminases, glycosylphosphate transferases, and phosphohydrolases. In total, there are 78 genes included in this database (Table S5). Based on the database, we conducted single-cell transcriptomic and proteomic studies to investigate the expression levels of FNC key phosphorylation kinases and the impact of FNC on the nucleotide metabolism system. The distribution of FNC in rat tissues was investigated, and it was found to be predominantly enriched in thymic tissue. Specifically, FNC-TP was only detected in the thymus and not detectable in other tissues. Single-cell transcriptomic data from the rat and rhesus monkey thymus demonstrated high expression levels of major phosphorylated kinases involved in cytidine analog FNC, namely Dck, Cmpk1, and Nme2, across major types of thymic cells including CD4+ T cells, DP cells, and CD8+ T cells (Fig. 7). Comparative analysis of gene expression changes with and without FNC administration among different types of thymic cells revealed that FNC could upregulate multiple phosphorylated kinases in cell types such as CD4+ T cells while downregulating the phosphatases and deaminases, respectively. Further investigations utilizing proteomics and PRM validation on thymus tissues of rats and rhesus monkeys have demonstrated the impact of FNC on the expression levels of various phosphorylation kinases, deaminases, phosphoribosyl transferases, and phosphohydrolases. The previous studies have revealed that FNC is the first dual-targeting nucleoside-based agent that inhibits nucleoside reverse transcriptase and restores expression of cytidine deaminase APOBEC3G (A3G) in HIV-1 patients derived CD4+ T cells[25]. The present study revealed a significant upregulation of various phosphorylation kinases associated with FNC activation in thymic immune cells, particularly in CD4+ T cells. The study of lymphocytes changing after SARS-CoV-2 infection in patients revealed that the CD4+, CD8+ T cell and NK cell were decreased, while DC, monocytes and macrophage progenitor cells were upregulated in blood[26]. According to our previous study, FNC treatment upregulated the proportion of CD4, CD8, and NKT cell type (CD4: 17.5% *vs.* 11.9%, CD8: 22.8% *vs.* 16.4%, NKT: 4.8% *vs.* 2%, compared to SARS-CoV-2 infection) in thymus, and that has been analyzed by single-cell RNA sequencing and demonstrated by multi-color immunofluorescent staining[26]. Meanwhile, based on the rat model study on virus infection, there were no significant alterations observed in the levels of CD4+ and CD8+ lymphocytes in both blood and liver following 28 days of rodent hepacivirus infection[27]. Therefore, the research about SARS-CoV-2 infection and FNC treatment in rat might be performed in future. Besides that, the circulating T cell count was associated with the progression of viral infection. The reduction of circulating CD4 T cell corresponded with delayed virus clearance of SARS-CoV-2 and disease severity[28,29]. The counts of circulating CD8 T cell were lower and the exhaustion was increased, which was associated with the progression of COVID-19[5]. In our previous study of FNC treatment in rhesus monkeys, the circulating T cell in PBMC were detected by flow cytometry after infection and FNC treated. The percentage of CD4 and CD8 T cells were significantly increased in 7 days after infection. These results indicated that the enhanced immune response in thymus by FNC treatment might influence the circulating T cell counts and promote the immune profile in general. In summary, thymic immune cells possess a robust phosphorylation capacity for cytidine analogues. Additionally, FNC demonstrated an activating effect on the nucleotide and nucleoside analogue metabolism system across

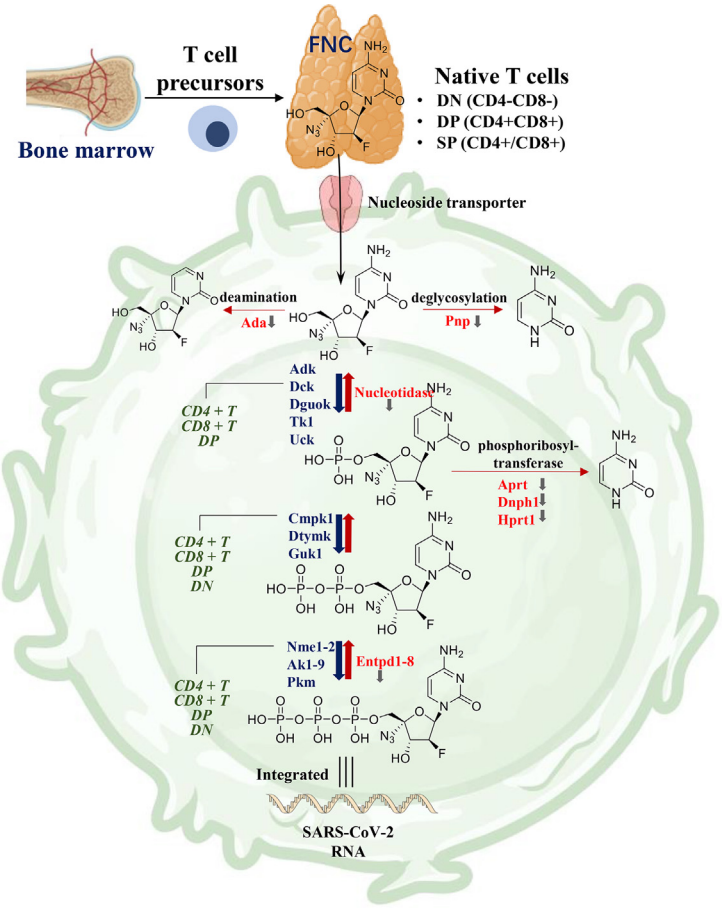

Figure 7 FNC demonstrated an activating effect on the nucleotide and nucleoside analogue metabolism system across diverse immune cell types within the thymus and activation of immune cells for anti-SARS-CoV-2 activity.

diverse immune cell types within the thymus, potentially contributing to its enrichment in thymic tissue and activation of immune cells for anti-SARS-CoV-2 activity (Fig. 7). Phosphorylation activation of FNC in the thymus might be significant attributed to its immunoprotective properties.

5. Conclusions

The present study revealed that single and multiple doses of the cytidine analogue FNC and its phosphorylated metabolites were mainly enriched in the thymus. The expression levels of cytidine analogue phosphorylating kinases Dck, Cmpk1, and Nme2 were high in the major types of immune cells in the thymus, indicating a strong phosphorylation ability of FNC on thymic cells. Furthermore, FNC could activate the nucleotide metabolism system of immune cells in the thymus, especially in CD4+ T cells. Taken together, these results indicate that FNC is enriched in thymic cells and efficiently metabolized into its triphosphorylated active form, activating immune cells and exerting anti-SARS-CoV-2 activity. These findings suggested that cytidine analogues might possess potential therapeutic advantages compared with other types of NAs following viral infection of T cells. Therefore, it is crucial to evaluate the expression level of NAs phosphorylated kinases when evaluating antiviral drug properties, as the phosphorylation activation ability of NAs represents an important factor for consideration during antiviral drug design.

Acknowledgments

We gratefully acknowledge financial support from the National Natural Science Foundation of China (No. 82151525; No. 82394460) and the National Key Research and Development Program of China (No. 2021YFC0864600).

Author contributions

Ning Sheng: Data curation, Formal analysis, Investigation, Methodology, Writing − original draft, Writing − review & editing, Visualization, Project administration. Rui Li: Data curation, Formal analysis, Writing − review & editing, Visualization. Yang Li: Formal analysis, Investigation. Zhe Wang: Formal analysis, Investigation. Lulu Wang: Investigation. Yuhuan Li: Investigation. Jinlan Zhang: Funding acquisition, Resources, Supervision. Jiandong Jiang: Funding acquisition, Resources, Supervision.

Conflicts of interest

The authors have declared that no competing interest exists.

Appendix A. Supporting information

Supporting information to this article can be found online at https://doi.org/10.1016/j.apsb.2024.03.032.

References

1. Klein L, Kyewski B, Allen PM, Hogquist KA. Positive and negative selection of the T cell repertoire: what thymocytes see (and don't see). *Nat Rev Immunol* 2014;**14**:377−91.
2. Huang M, Pan X, Wang X, Ren Q, Tong B, Dong X, et al. Lymphocyte integrins mediate entry and dysregulation of T cells by SARS-CoV-2. *Signal Transduct Target Ther* 2023;**8**:84.
3. Shen XR, Geng R, Li Q, Chen Y, Li SF, Wang Q, et al. ACE2-independent infection of T lymphocytes by SARS-CoV-2. *Signal Transduct Target Ther* 2022;**7**:83.
4. Li M, Guo W, Dong Y, Wang X, Dai D, Liu X, et al. Elevated exhaustion levels of NK and CD8+ T cells as indicators for progression and prognosis of COVID-19 disease. *Front Immunol* 2020;**11**:580237.
5. Yang PH, Ding YB, Xu Z, Pu R, Li P, Yan J, et al. Increased circulating level of interleukin-6 and CD8+ T cell exhaustion are associated with progression of COVID-19. *Infect Dis Poverty* 2020;**9**:161.
6. Zhang JL, Li YH, Wang LL, Liu HQ, Lu SY, Liu Y, et al. Azvudine is a thymus-homing anti-SARS-CoV-2 drug effective in treating COVID-19 patients. *Signal Transduct Target Ther* 2021;**6**:414.
7. Zong K, Zhou H, Li W, Jiang E, Liu Y, Li S. Azvudine reduces the in-hospital mortality of COVID-19 patients: a retrospective cohort study. *Acta Pharm Sin B* 2023;**13**:4655−60.
8. Roy B, Navarro V, Peyrottes S. Prodrugs of nucleoside 5′-monophosphate analogues: overview of the recent literature concerning their synthesis and applications. *Curr Med Chem* 2023;**30**:1256−303.
9. Yu B, Chang J. The first Chinese oral anti-COVID-19 drug Azvudine launched. *Innovation (Camb)* 2022;**3**:100321.
10. Ren Z, Luo H, Yu Z, Song J, Liang L, Wang L, et al. A randomized, open-label, controlled clinical trial of Azvudine tablets in the treatment of mild and common COVID-19, a pilot study. *Adv Sci* 2020;**7**:e2001435.
11. Van Rompay AR, Johansson M, Karlsson A. Phosphorylation of nucleosides and nucleoside analogs by mammalian nucleoside monophosphate kinases. *Pharmacol Ther* 2000;**87**:189−98.
12. Deville-Bonne D, El Amri C, Meyer P, Chen Y, Agrofoglio LA, Janin J. Human and viral nucleoside/nucleotide kinases involved in antiviral drug activation: structural and catalytic properties. *Antiviral Res* 2010;**86**:101−20.
13. Li R, Liclican A, Xu Y, Pitts J, Niu C, Zhang J, et al. Key Metabolic enzymes involved in Remdesivir activation in human lung cells. *Antimicrob Agents Chemother* 2021;**65**:e0060221.
14. Austin WR, Armijo AL, Campbell DO, Singh AS, Hsieh T, Nathanson D, et al. Nucleoside salvage pathway kinases regulate hematopoiesis by linking nucleotide metabolism with replication stress. *J Exp Med* 2012;**209**:2215−28.
15. Perez-Riverol Y, Bai J, Bandla C, García-Seisdedos D, Hewapathirana S, Kamatchinathan S, et al. The PRIDE database resources in 2022: a hub for mass spectrometry-based proteomics evidences. *Nucleic Acids Res* 2022;**50**:D543−52.
16. Björkström NK, Strunz B, Ljunggren HG. Natural killer cells in antiviral immunity. *Nat Rev Immunol* 2022;**22**:112−23.
17. Pao LI, Sumaria N, Kelly JM, van Dommelen S, Cretney E, Wallace ME, et al. Functional analysis of granzyme M and its role in immunity to infection. *J Immunol* 2005;**175**:3235−43.
18. Bardina SV, Brown JA, Michlmayr D, Hoffman KW, Sum J, Pletnev AG, et al. Chemokine receptor Ccr7 restricts fatal West Nile virus encephalitis. *J Virol* 2017;**91**:e02409−16.
19. Bordoni V, Tartaglia E, Sacchi A, Fimia GM, Cimini E, Casetti R, et al. The unbalanced p53/SIRT1 axis may impact lymphocyte homeostasis in COVID-19 patients. *Int J Infect Dis* 2021;**105**:49−53.
20. Kondo K, Ohigashi I, Takahama Y. Thymus machinery for T-cell selection. *Int Immunol* 2019;**31**:119−25.
21. Jordheim LP, Durantel D, Zoulim F, Dumontet C. Advances in the development of nucleoside and nucleotide analogues for cancer and viral diseases. *Nat Rev Drug Discov* 2013;**12**:447−64.
22. Ray AS, Hostetler KY. Application of kinase bypass strategies to nucleoside antivirals. *Antiviral Res* 2011;**92**:277−91.
23. Jordan PC, Stevens SK, Tam Y, Pemberton RP, Chaudhuri S, Stoycheva AD, et al. Activation pathway of a nucleoside analog inhibiting respiratory syncytial virus polymerase. *ACS Chem Biol* 2017;**12**:83−91.
24. Anderson PL, Kakuda TN, Lichtenstein KA. The cellular pharmacology of nucleoside- and nucleotide-analogue reverse-transcriptase inhibitors and its relationship to clinical toxicities. *Clin Infect Dis* 2004;**38**:743−53.
25. Sun L, Peng Y, Yu W, Zhang Y, Liang L, Song C, et al. Mechanistic insight into antiretroviral potency of 2′-deoxy-2′-β-fluoro-4′-azidocytidine (FNC) with a long-lasting effect on HIV-1 prevention. *J Med Chem* 2020;**63**:8554−66.
26. Atcheson E, Li W, Bliss CM, Chinnakannan S, Heim K, Sharpe H, et al. Use of an outbred rat hepacivirus challenge model for design and evaluation of efficacy of different immunization strategies for hepatitis C virus. *Hepatology* 2020;**71**:794−807.
27. Huang L, Shi Y, Gong B, Jiang L, Zhang Z, Liu X, et al. Dynamic blood single-cell immune responses in patients with COVID-19. *Signal Transduct Target Ther* 2021;**6**:110.
28. Zlei M, Sidorov IA, Joosten SA, Heemskerk MHM, Myeni SK, Pothast CR, et al. Immune determinants of viral clearance in hospitalised COVID-19 patients: reduced circulating naïve CD4+ T cell counts correspond with delayed viral clearance. *Cells* 2022;**11**:2743.
29. Caldrer S, Mazzi C, Bernardi M, Prato M, Ronzoni N, Rodari P, et al. Regulatory T cells as predictors of clinical course in hospitalised COVID-19 patients. *Front Immunol* 2021;**12**:789735.